Acta Crystallographica Section D
Biological Crystallography
ISSN 0907-4449

Structural insight into the ISC domain of VibB from *Vibrio cholerae* at atomic resolution: a snapshot just before the enzymatic reaction

Shiheng Liu,[a]‡ Conggang Zhang,[a]‡ Ning Li,[a] Bei Niu,[a] Mengyuan Liu,[b] Xiuhua Liu,[c] Tiandi Wei,[a] Deyu Zhu,[a] Yan Huang,[a] Sujuan Xu[a] and Lichuan Gu[a]*

[a]State Key Laboratory of Microbial Technology, Shandong University, 27 Shanda Nanlu, Jinan, Shandong 250100, People's Republic of China, [b]State Key Laboratory of Crystal Materials, Shandong University, 27 Shanda Nanlu, Jinan, Shandong 250100, People's Republic of China, and [c]College of Life Sciences, Hebei University, 180 Wusi Donglu, Baoding, Hebei 071002, People's Republic of China

‡ These authors contributed equally to this work.

Correspondence e-mail: lcgu@sdu.edu.cn

Received 6 February 2012
Accepted 23 June 2012

PDB References: VibB ISC domain, 3tb4; complex with isochorismate, 3tg2

The N-terminal isochorismatase (ISC) domain of VibB (VibB-ISC) catalyzes the vinyl ether hydrolysis of isochorismate to 2,3-dihydro-2,3-dihydroxybenzoate and pyruvate. Structures of the ISC domain and its complex with isochorismate have been determined at 1.35 and 1.10 Å resolution, respectively. Two catalytic waters which were absent from previously reported homologous structures were observed adjacent to isochorismate and the catalytic residues (Asp35 and Lys118) in the VibB-ISC complex. Molecular-dynamics (MD) simulations starting with the structure of the VibB-ISC complex suggest that the catalytic waters contribute to the hydrolysis of the vinyl ether by participating in two reactions. Firstly, they may function as a general acid to protonate the Asp35 carboxylate prior to isochorismate protonation; secondly, one of the catalytic waters may be activated by the ionizable side chain of Asp35 to perform a nucleophilic attack on the intermediate carbocation/oxocarbonium ion. The positions of the waters are both significantly affected by the mutation of Asp35 and Lys118. The structural, biochemical and MD results reveal the residues that are involved in substrate binding and provide clues towards defining a possible mechanism.

1. Introduction

Siderophore-dependent iron acquisition is universally related to virulence mechanisms of microbes that are pathogenic to both animal and plants (Miethke & Marahiel, 2007; Neilands, 1995). In *Vibrio cholerae*, the catechol siderophore vibriobactin is synthesized by nonribosomal peptide synthetases (NRPSs; Fig. 1) in order to efficiently acquire iron from animal hosts and the environment (Griffiths *et al.*, 1984). In the process of vibriobactin biosynthesis, VibABC is required to produce 2,3-dihydroxybenzoate (2,3-DHB) from chorismate (Wyckoff *et al.*, 1997) and VibBDEFH is required to assemble vibriobactin from 2,3-DHB, threonine and norspermidine (Keating *et al.*, 2000). Previous studies have shown that mutations in any of the vibriobactin-biosynthetic genes can inhibit vibriobactin biosynthesis, indicating that NRPSs might serve as therapeutic targets for human infections caused by *V. cholerae* (Wyckoff *et al.*, 1997, 2001; Butterton *et al.*, 2000).

The NRPS VibB encodes a 293-amino-acid protein with an N-terminal isochorismatase (ISC) domain and a C-terminal aryl carrier protein (ArCP) domain. The ISC domain of VibB is believed to catalyze the hydrolysis of isochorismate to 2,3-dihydro-2,3-DHB and pyruvate (Fig. 1). Some proteins that are homologous to the VibB ISC domain, such as the

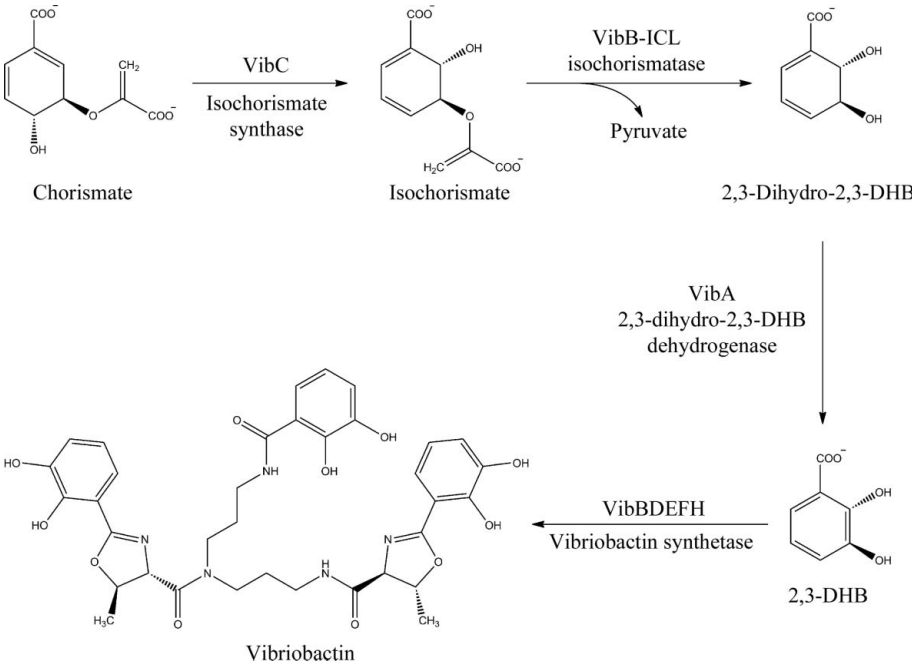

Figure 1
Biosynthetic pathway of vibriobactin in *V. cholerae*; adapted from Wyckoff *et al.* (1997) and Keating *et al.* (2000).

EntB ICL domain (EntB-ICL) from *Escherichia coli* involved in enterobactin biosynthesis and PhzD from *Pseudomonas aeruginosa* involved in phenazine biosynthesis, also have isochorismatase activity (Rusnak *et al.*, 1990; Parsons *et al.*, 2003).

The hydrolysis of a vinyl ether catalyzed by isochorismatases is an uncommon reaction in biological systems (Rusnak *et al.*, 1990; Kresge *et al.*, 1992). Based on the mechanism of the hydrolysis of vinyl ethers that has been well characterized in solution (Wibbenmeyer *et al.*, 1988), a general catalytic system for isochorismate has been proposed. To date, crystal structures of the VibB-ISC homologues PhzD (PDB entries 1nf8 and 1nf9; 1.6 and 1.5 Å resolution, respectively) and EntB-ICL (PDB entry 2fq1; 2.3 Å resolution) have been determined (Parsons *et al.*, 2003; Drake *et al.*, 2006). According to the structure of the PhzD–substrate complex, Asp38 was identified as the general acid that protonates C3′ of isochorismate. However, water molecules were not observed in the active site in this structure. It remains unclear how Asp38 is protonated and how the catalytic water molecules perform a nucleophilic attack on the intermediate carbocation/oxocarbonium ion.

In order to elucidate the mechanism of isochorismate hydrolysis catalyzed by VibB-ISC, we determined the crystal structure of VibB-ISC and of its catalytic mutant (D35N) in complex with isochorismate at 1.35 and 1.10 Å resolution, respectively. As expected, two catalytic waters which were absent in the previous reported homologous structure (PDB entry 1nf9) were observed adjacent to isochorismate and the catalytic residues (Asp35 and Lys118) in our structures. Combined with molecular-dynamics (MD) simulations, our structures suggest a mechanism which is supported by the results of site-directed mutagenesis and phenotype analysis.

2. Materials and methods

2.1. Cloning, site-directed mutagenesis, protein expression and purification

Sequences encoding the isochorismatase domain (residues 1–215) of VibB were amplified by PCR using genomic DNA isolated from *V. cholerae* O1 biovar El Tor strain N16961. The PCR product was cloned into the *Nde*I and *Xho*I sites of pET-21b (Novagen) and the plasmid was overexpressed in *E. coli* strain BL21 (DE3). Based on sequence alignment and the structure of the VibB-ISC complex, the following mutations were designed: D35N, K118H, K118N, K118A, H34N and H34A. Mutations were carried out by a two-step PCR strategy and were confirmed by DNA sequencing.

For protein purification, 2 l of bacteria was incubated in lactose broth at 310 K to an absorbance (A_{600}) of 0.8. Following overnight induction with 0.12 m*M* isopropyl β-D-1-thiogalactopyranoside at 288 K, the cells were harvested at 4200 rev min^{-1} for 15 min at 277 K. The resulting bacteria were suspended in 25 m*M* Tris–HCl buffer pH 8.0 containing 200 m*M* NaCl and lysed by sonication. After ultracentrifugation at 14 000 rev min^{-1} for 45 min at 277 K, the supernatant was loaded onto an Ni^{2+} Chelating Sepharose Fast Flow column (GE Healthcare) for affinity chromatography of the C-terminal His_6-tagged VibB-ISC and eluted with 25 m*M* Tris–HCl buffer pH 8.0 containing 100 m*M* NaCl and 250 m*M* imidazole. The sample buffer was then loaded onto an ion-exchange column (Source 15Q, GE Healthcare) and eluted with a linear gradient of 0–1 *M* NaCl in 25 m*M* Tris–HCl buffer pH 8.0. Finally, the protein sample was purified by size-exclusion chromatography (Superdex 200, GE Healthcare) with 10 m*M* Tris–HCl buffer pH 8.0 containing 100 m*M* NaCl and 0.3 m*M* dithiothreitol.

2.2. Crystallization of VibB-ISC in the presence and absence of isochorismate

For crystallization, both VibB-ISC and the D35N mutant were concentrated to 10 mg ml^{-1} in 10 m*M* Tris–HCl pH 8.0, 100 m*M* NaCl, 0.3 m*M* dithiothreitol. Crystals of wild-type VibB-ISC were initially obtained by sitting-drop vapour diffusion at 293 K. After optimization, diffraction-quality rod-like crystals were grown in hanging drops by mixing equal volumes of protein solution and reservoir solution [50 m*M* $CaCl_2$, 0.1 *M* bis-Tris pH 6.5, 28%(*w*/*v*) polyethylene glycol monomethyl ether 550, 1%(*w*/*v*) *n*-octyl-β-D-glucoside] at 293 K. To obtain crystals with isochorismate, concentrated D35N mutant was mixed with 40 m*M* $MgCl_2$, 2.4 m*M* chorismate and 0.02 mg ml^{-1} EntC (isochorismate synthase from

Table 1
Data-collection and refinement statistics.

Values in parentheses are for the highest resolution shell.

	Ligand-bound VibB-ISC	Wild-type VibB-ISC
Beamline	SSRF	BSRF
Space group	$P3_221$	$P3_221$
Unit-cell parameters (Å)	$a = b = 55.58$, $c = 119.79$	$a = b = 55.66$, $c = 118.75$
Wavelength (Å)	0.9792	0.9792
Resolution (Å)	50.00–1.10 (1.12–1.10)	50–1.35 (1.40–1.35)
Measured reflections	1336261 (18088)	506929 (42551)
Unique reflections	87374 (4111)	47657 (4676)
$\langle I/\sigma(I)\rangle$	40.03 (2.19)	45.81 (3.48)
Completeness (%)	99.7 (95.0)	99.9 (100)
Multiplicity	15.3 (4.4)	10.6 (9.1)
$R_{\rm merge}$† (%)	6.9 (52.8)	5.4 (48.6)
Wilson B factor (Å^2)	10.37	13.78
Solvent content (%)	42.8	42.4
$R_{\rm work}$ (%)	12.72	13.42
$R_{\rm free}$ (%)	14.44	16.62
No. of atoms		
Protein (non-H/H)	1698/1747	1678/1708
Ligand (non-H/H)	26/22	41/58
Ion	—	1
Solvent	265	280
R.m.s.d. from ideal geometry		
Bond lengths (Å)	0.009	0.010
Bond angles (°)	1.412	1.317
Average B factors (Å^2)		
Protein	15.3	18.2
Ligand	21.4	33.7
Ion	—	15.4
Solvent	27.9	33.0
Anisotropy (%)		
Mean	55.2	38.5
Standard deviation	13.7	13.0
Ramachandran plot (%)		
Favoured	92.7	92.7
Allowed	7.3	7.3

† $R_{\rm merge} = \sum_{hkl}\sum_i |I_i(hkl) - \langle I(hkl)\rangle| / \sum_{hkl}\sum_i I_i(hkl)$, where $\langle I(hkl)\rangle$ is the mean intensity of multiply recorded reflections.

E. coli O157) for 5 min at room temperature and 20 min on ice prior to crystallization. Double conical crystals were obtained under the same conditions as those used for wild-type VibB-ISC but in the absence of *n*-octyl-β-D-glucoside in the reservoir solution. Reservoir solution supplemented with 15–20% glycerol was used as a cryoprotectant in all cases and all data sets were collected at 100 K in a nitrogen stream.

2.3. Data collection, processing and structure determination

Crystals were cryoprotected by supplementing the mother liquor with 15–20%(*v*/*v*) glycerol and flash-cooled in liquid nitrogen. X-ray diffraction data were collected at 100 K on beamline 3W1A at BSRF, Beijing, People's Republic of China equipped with a MAR CCD 165 detector or on beamline BL17U at SSRF, Shanghai, People's Republic of China equipped with a MAR Mosaic CCD 225 detector.

The data were integrated and scaled using the *HKL*-2000 program suite (Otwinowski & Minor, 1997). The calculated Matthews coefficient ($V_{\rm M}$; Matthews, 1968) of 2.14 Å^3 Da^{-1} for wild-type VibB-ISC indicated the presence of one monomer per asymmetric unit, corresponding to a solvent content of 42.4%. The 1.35 Å resolution structure of wild-type VibB-ISC was solved by molecular replacement using *Phaser* from the *CCP*4 suite of programs (McCoy *et al.*, 2007; Winn *et al.*, 2011) with the ICL domain (residues 4–205) of EntB (PDB entry 2fq1) as the search model. The resulting density map exhibited clear features such as helices, strands and even some side chains. The initial model of the wild-type protein was built by *ARP*/*wARP* (Lamzin & Wilson, 1993) and further refined using *phenix.refine* (Adams *et al.*, 2002) with additional rounds of manual rebuilding using the *Coot* molecular-graphics program (Emsley & Cowtan, 2004). In the final steps of refinement, H atoms were added to the ligand structure using *phenix.reduce* (Word *et al.*, 1999) and refined as a riding model. Water molecules were added by *phenix.refine* for peaks higher than 3.0σ in the $mF_{\rm o} - DF_{\rm c}$ map. The resulting water molecules were finally checked for hydrogen bonding in *Coot* and modified if necessary. An additional refinement step, including a final individual ADP refinement (Grosse-Kunstleve & Adams, 2002) using isotropic waters and H atoms while the other atoms were refined as anisotropic was carried out with *PHENIX*. The final R values were $R_{\rm work}$ = 13.4% and $R_{\rm free}$ = 16.6% based on a subset of 4.2% of the reflections. The high-resolution ligand structure (1.10 Å) was subsequently solved using the refined wild-type PDB model as a reference in *Phaser*. An isochorismate was added to the model by *Coot* based on the $mF_{\rm o} - DF_{\rm c}$ density map of the ligand structure. The same refinement was carried out as for the wild-type structure. The final R factors were $R_{\rm work}$ = 12.7% and $R_{\rm free}$ = 14.4% based on a subset of 2.3% of the reflections.

X-ray diffraction data-collection and refinement statistics are presented in Table 1. The final model was checked and validated using *PROCHECK* (Laskowski *et al.*, 1993), *QMEAN* (Benkert *et al.*, 2008) and *ProQ* (Cristobal *et al.*, 2001), which indicated a good-quality model (Table 1 and Supplementary Table S3[1]). All residues were within allowed regions of the Ramachandran plot (Ramachandran & Sasisekharan, 1968). The mean temperature factors for protein and solvent were calculated using *BAVERAGE* from the *CCP*4 program suite (Winn *et al.*, 2011). Anisotropic refinement analysis was performed with *PARVATI* (Merritt, 1999).

The atomic coordinates and structure factors of wild-type VibB-ISC and isochorismate-bound VibB-ISC have been deposited in the Protein Data Bank with accession codes 3tb4 and 3tg2, respectively.

2.4. Enzyme assays

Measurement of the activity of VibB-ISC was performed in two steps. Firstly, EntC was used to convert chorismate to isochorismate. The conversion was performed in a total volume of 100 µl containing 20 m*M* chorismate, 100 m*M* PBS buffer pH 7.0, 10 m*M* $MgCl_2$ and 0.85 µg purified EntC at

[1] Supplementary material has been deposited in the IUCr electronic archive (Reference: DW5016). Services for accessing this material are described at the back of the journal.

room temperature for 2 h. Next, the VibB-ISC activity was analyzed in a coupled assay with VibA (2,3-dihydro-2,3-DHBA dehydrogenase from *V. cholerae* O1 biovar El Tor strain N16961) by observing the increase in absorbance at 340 nm owing to NAD^+ reduction in an Uvikon spectrophotometer. The assay was performed in a total volume of 50 µl containing 5 µl reaction solution from the first step, 100 m*M* PBS buffer pH 7.0, 0.8 m*M* NAD^+, 0.06 µg purified VibB-ISC and 3.8 µg purified VibA at room temperature.

2.5. Phenotype analysis of *vibB-ISC* mutants using Δ*entB-ICL* strain

The *entB-ICL* gene was deleted from the *E. coli* BL21 (DE3) genome using the Red recombinase system described by Datsenko & Wanner (2000). Briefly, K1 and K2 oligonucleotides (Supplementary Table S1) were used for PCR amplification of the kanamycin-resistance gene from pKD4 flanked by sequences designed for specific disruption of the *entB-ICL* gene. The PCR product was transformed by electroporation into *E. coli* BL21 (DE3) (pKD46) expressing Red recombinase and recombinant clones were isolated on a kanamycin-resistant LB plate. The *entB*::*kan* genotype was ensured by PCR using K3 and K4 as primers (Supplementary Table S1).

The plasmid for the expression of the *entB-ICL* gene was constructed (Supplementary Table S1). This gene was amplified by PCR using genomic DNA isolated from *E. coli* O157:H7. The PCR product was cloned into the *Nde*I and *Xho*I sites of pET-21b (Novagen) and transformed into *E. coli* strain BL21 (DE3). Plasmids for the expression of the *vibB-ISC*, *vibB-ISC-K118N*, *vibB-ISC-K118H*, *vibB-ISC-K118A* and *vibB-ISC-D35N* genes were all constructed similarly (Supplementary Table S1). The details have been provided above.

Phenotype analysis of *vibB-ISC* mutants was performed on an LB plate with or without 2,2-bipyridyl. A total of 500 µl of bacteria was incubated at 310 K in lactose broth for 5 h. Cells were harvested at 3000 rev min^{-1} for 2 min at 277 K and then washed twice with 500 µl sterile water. The resulting bacteria were suspended in 5 ml sterile water. 1 µl of bacteria was spotted onto a LB plate by pipette and cultured at 310 K for 48 h.

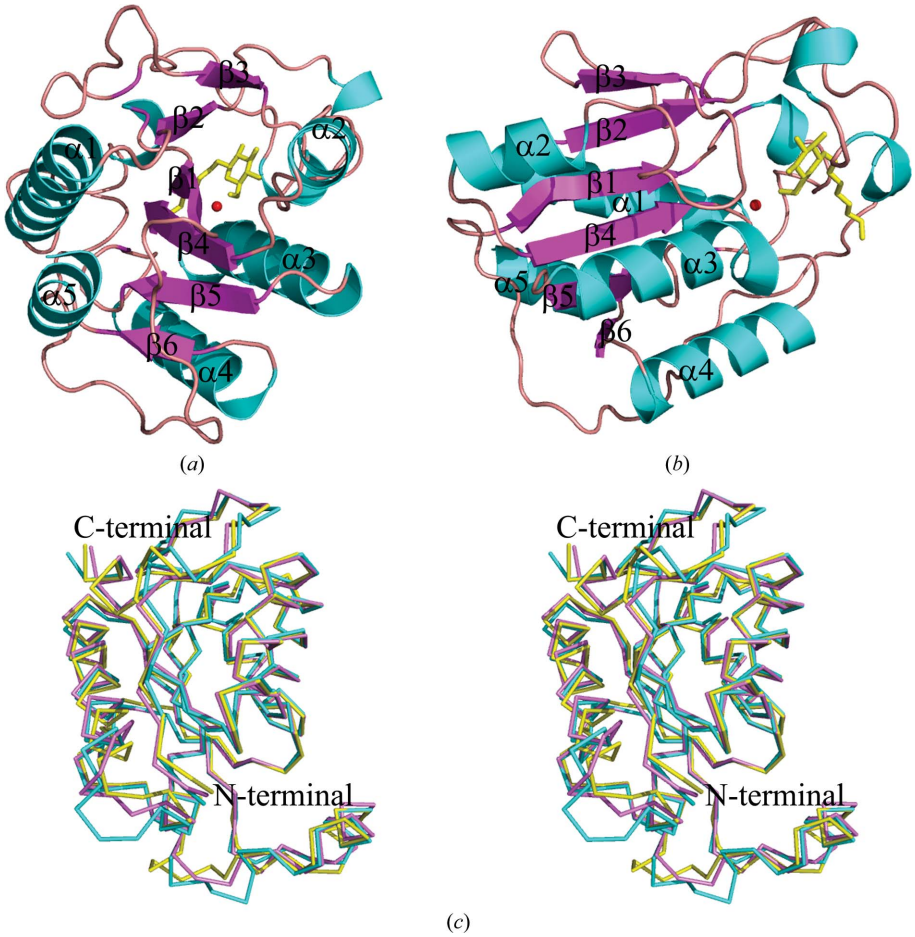

Figure 2
Overall structure of wild-type VibB-ISC. (*a*, *b*) Cartoon representation of wild-type VibB-ISC in two different views. α-Helices and β-strands are shown in cyan and purple, respectively. *N*-Octyl-β-D-glucoside is shown in yellow. (*c*) Stereoview of a ribbon representation showing C^α superposition of VibB-ISC with PhzD and EntB-ICL. PhzD and EntB-ICL are shown in yellow and cyan, respectively; VibB-ISC is shown in purple. All structural representations were generated using *PyMOL* (http://www.pymol.org).

2.6. MD simulation

The simulations were based on the 1.10 Å resolution crystal structure of the D35N mutant of VibB-ISC in complex with isochorismate. Initial models were constructed for MD simulation of the wild-type VibB-ISC complex structure and its K118A, K118H and K118N mutants. The K118A mutant was generated by replacing the side chain of Lys with an H atom in the wild-type structure. Other mutants were obtained by replacing the original side chain with a corresponding side chain in a similar orientation. All water molecules were deleted from the initial models except for WAT1 and WAT2, which are located in the active site of the protein (Fig. 4*b*).

The initial protein structures were hydrogenized and solvated with rigid SPC waters (Berendsen *et al.*, 1981) in a periodically replicated cubic box using the *Protein Preparation Wizard* and *System Builder* utilities in *Maestro* (Schrödinger LLC, New York, USA), respectively. The net charge of the system was neutralized using sodium or chloride ions. The random placement of Na^+ and Cl^- ions in the bulk solvent was carried out using the *System Builder* utility of *Maestro* (Schrödinger LLC).

MD simulations of wild-type VibB-ISC and its mutants were performed using *Desmond* v.2.2 and the OPLS2001 force field (Bowers *et al.*, 2006). Long-range electrostatic interactions were calculated using the Smooth Particle Mesh Ewald method with a cutoff of 9.0 Å (Darden *et al.*, 1993) and all bonds were constrained using the *SHAKE* algorithm (Ryckaert *et al.*, 1977). All models first underwent relaxation including energy minimization and a 1 ns MD simulation. Another 1 ns MD simulation was then performed for each system at 300 K in the NPT ensemble, saving all MD trajectories at a time step of 4.8 ps. A Nosé–Hoover thermostat (Nosé, 1984; Hoover, 1985) was applied to maintain constant temperature. The trajectories generated from the NVT runs were used in further data analysis.

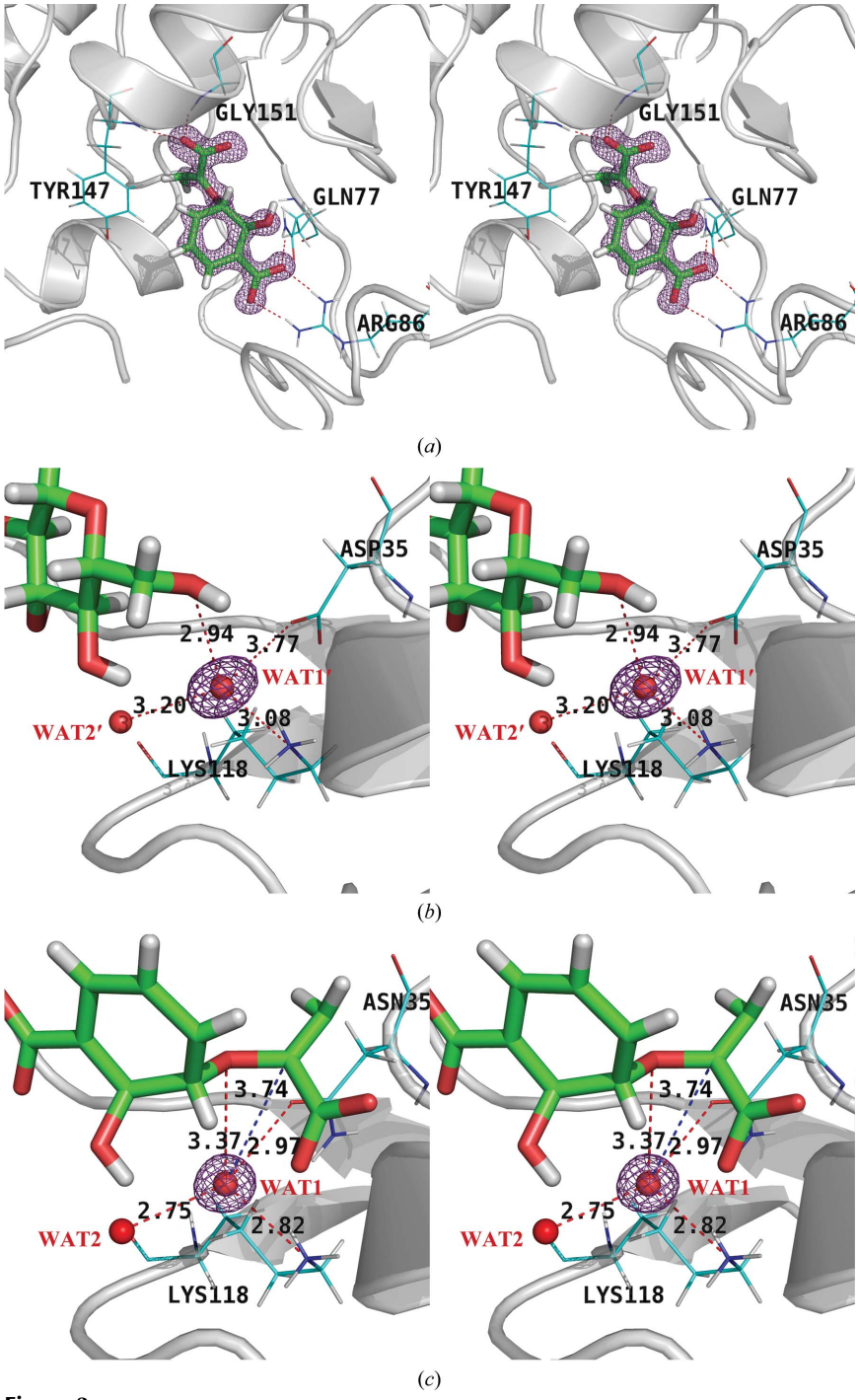

Figure 3
Structures of the active site. (*a*) Stereoview of the isochorismate-bound structure in the active site. An $F_o - F_c$ OMIT map contoured at 4.5σ shows electron density for isochorismate. Amino-acid residues forming hydrogen bonds (red dashed lines) to the substrate are indicated. (*b*, *c*) Putative catalytic water (WAT1′ or WAT1) and catalytic side chains in the active site from crystal structures. An $F_o - F_c$ OMIT map contoured at 4.5σ shows electron density for the putative catalytic water. Amino-acid residues and another water molecule (WAT2′ or WAT2) forming hydrogen bonds (red dashed lines) to the catalytic water are indicated. (*b*) represents the complex structure with isochorismate (ISC); the blue dashed line indicates a distance of 3.74 Å between the catalytic water and isochorismate C2′. (*c*) represents the wild-type structure with *n*-octyl-β-D-glucoside (BOG).

3. Results

3.1. Overall structure of VibB-ISC

The final model shows that each asymmetric unit contains one monomer. All atoms of the model are well defined except for two disordered amino-acid residues at the N-terminus and eight at the C-terminus. The monomer of VibB-ISC reveals a globular and α/β mixed scaffold which contains a six-stranded parallel β-sheet (3–2–1–4–5–6) sandwiched by three α-helices (2–3–4) on one side and two α-helices (1 and 5) on the other (Figs. 2*a* and 2*b*). The other portion of the protein is mainly comprised of unstructured loops, in which residues Gln77–Leu97 participate in formation of the active-site pocket. Two *cis*-peptide bonds (Glu49-Pro50 and Val146-Tyr147) are present in the structure. The Val146-Tyr147 *cis*-peptide bond is important in the construction of the catalytic site.

The scaffold of VibB-ISC is highly conserved across all known isochorismatase structures. A structural alignment was carried out using the *DALI* program (Holm & Sander, 1993). Similarity searches against the PDB show that the PhzD structure is most similar to that of VibB-ISC (*Z*-score 33.9), followed by EntB (*Z*-score 33.6), PSPPH_2384 (*Z*-score 26.7) and CHSase (*Z*-score 25.9). C^{α} superposition of VibB-ISC with PhzD and EntB-ICL yielded root-mean-square deviations (r.m.s.d.s) of 0.667 and 0.622 Å, respectively (Fig. 2*c*). This suggests that the scaffold of these proteins is necessary for creating the geometry of the ligand-binding site. At the same time, VibB-ISC also exists as a stable dimer in solution

like its homologue. Crystal-packing analysis shows that each polypeptide chain in the asymmetric unit forms a conserved dimer with a symmetry-related adjacent molecule.

3.2. Isochorismate-complex structure

The D35N structure is essentially identical to the wild-type structure. The $F_{obs} - F_{calc}$ map clearly shows the existence of isochorismate in the active site located close to the C-terminus of VibB-ISC (Fig. 3*a*). Interactions between isochorismate and VibB-ISC are mainly mediated by waters or by direct hydrogen bonds (Fig. 3*a*). Such interactions have also been found in the active sites of PhzD (Parsons *et al.*, 2003). Some residues, including Ile3, Phe40, Leu89, Trp93, Tyr121, Val146, Tyr147, Ile150 and Phe176, form a hydrophobic pocket around the substrate. All of these hydrophobic residues are conserved according to the multiple sequence alignment shown in Fig. 4(*a*). The *cis*-peptide bond between Val146 and Tyr147 is functionally important for the correct positioning of Tyr147 and Gly151, which participate in the formation of hydrogen bonds to isochorismate. The *cis*-peptide bond has also been found in the structures of VibB-ISC homologues (Parsons *et al.*, 2003; Drake *et al.*, 2006), indicating that a *cis* conformation of the protein backbone is necessary to create the geometry of the active site.

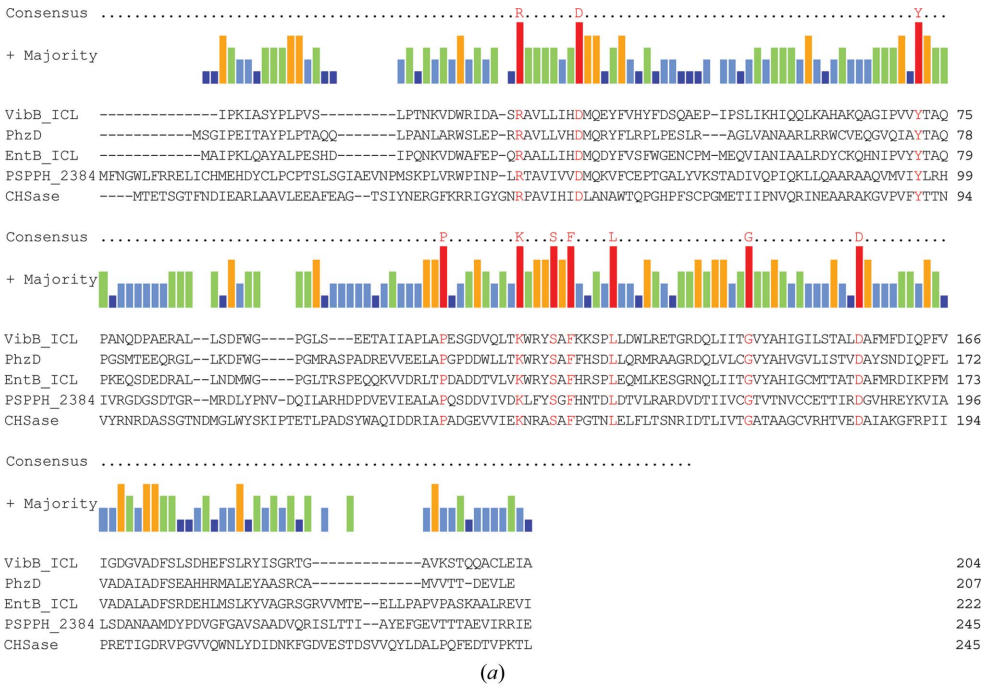

(*a*)

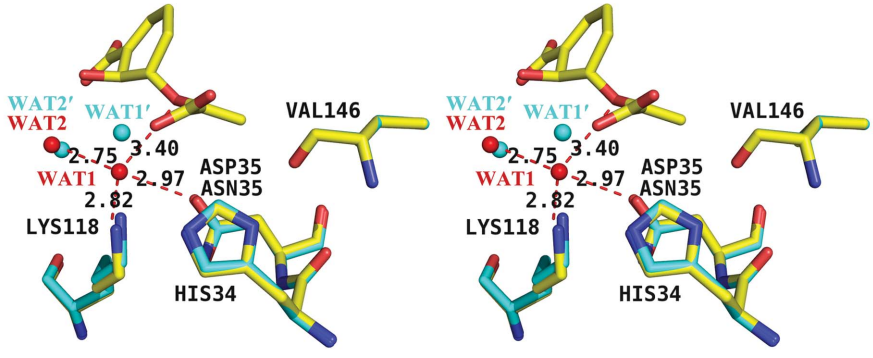

(*b*)

Figure 4
Catalytic residues in the active site. (*a*) Multiple sequence alignment of VibB-ISC from *V. cholerae*, PhzD (isochorismatase; PDB entry 1nf9) from *P. aeruginosa*, EntB-ICL (isochorismatase; PDB entry 2fq1) from *E. coli*, PSSPPH_2384 (cysteine hydrolase; PDB entry 3irv; New York SGX Research Center for Structural Genomics, unpublished work) from *P. syringae* pv. phaseolicola 1448A and CHSase (*N*-carbamoylsarcosine amidohydrolase; PDB entry 1nba; Romão *et al.*, 1992) from *Arthrobacter* sp. The alignment was carried out using *MegAlign* (http://www.dnastar.com/t-sub-products-lasergene-megalign.aspx). 'Majority' shows the histogram of consensus strength. The residues conserved in all five sequences are highlighted in red. (*b*) Stereoview of active-site residues from the two superimposed VibB-ISC structures. Wild-type and complex structures are shown in cyan and yellow, respectively. The water molecules in the active site are represented as spheres. WAT1′ and WAT1 represent the putative catalytic water in the wild-type and complex structures, respectively. WAT2′ and WAT2 represent an additional water molecule that forms hydrogen bonds to the catalytic water in the wild-type and complex structures, repectively. The hydrogen bonds between WAT1 and residues in the complex structure are shown as red dashed lines.

The substrate binding in the active site was shown to be the (+)-2*S*,3*S* isomer of isochorismate (Fig. 3*a*), suggesting that only one enantiomer is metabolized by the enzyme. This is consistent with characterization of the isolated isochorismate and EntB enzyme assays (Young *et al.*, 1969; Rusnak *et al.*, 1990). The side chain of D35N approaches the C3′ of isochorismate from the *re* face of C2′. The side chain of D35N has the same orientation as D38A in the PhzD complex structure, indicating that the stereochemistry for vinyl ether hydrolysis of isochorismate should be substantially similar. C3′ of isochorismate is 3.43 Å away from D35N. It is consistent with a mechanism in which the proton is transferred directly from the side chain of Asp35 to the C3′ of isochorismate.

3.3. Waters in the active site

Water molecules are necessary for the activity of all hydrolases. The positioning of water molecules in the enzyme active site is very important for clarifying the catalytic mechanism. However, in the D38A PhzD structure (PDB entry 1nf8) no water molecules were observed adjacent to the catalytic residues. It remains unclear how water molecules play a role in the enzymatic hydrolysis of isochorismate. In our structure,

a water molecule (WAT1; Fig. 3*c*) was observed between isochorismate and several residues of the active site which was suitable for direct nucleophilic attack on the C2′ atom of the substrate. The putative catalytic water (WAT1; Fig. 4*b*) in the complex structure is 2.97 Å away from D35N, suggesting that the proton transfers directly from the water to the Asp35 carboxyl group before the protonation of isochorismate. The amino group of Lys118 in the complex structure is within 2.82 Å of the putative catalytic water (WAT1; Fig. 4*b*). The Lys118 stays in a position that allows it to function as a general base to activate the water molecule. Another water molecule (WAT2 or WAT2′) observed in both structures forms a hydrogen-bonding interaction with the putative catalytic water (WAT1 or WAT1′), indicating that it might be indispensable for the stabilization of the catalytic water. However, the dynamic analysis shows that this water molecule (WAT2 or WAT2′) might also shift into a suitable position to function as a general acid for protonation of Asp35.

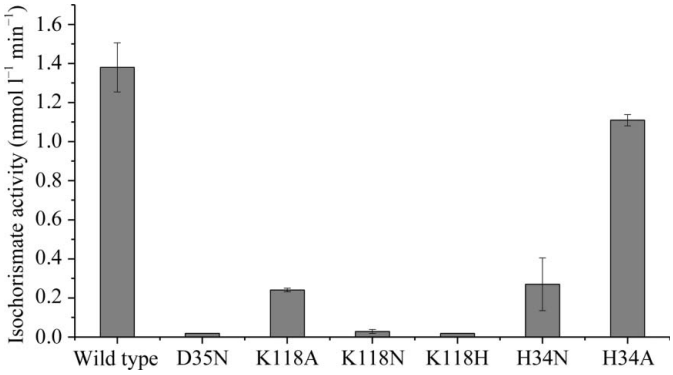

Figure 5
Effect of active-site residue mutants on the isochorismatase activity of VibB-ISC. Activity is defined as micromoles of NAD reduced per minute per millitre in the VibA coupled assay after subtracting NAD reduced activity in the absence of VibB. Error bars indicate standard deviations. All enzyme-activity figures were drawn using *OriginPro* 8.

3.4. Exploring the active-site residues by site-directed mutagenesis

Structural analysis indicates that only Asp35, Lys118 and His34 might participate in the process of vinyl ether hydrolysis (Fig. 4*b*). These three residues are conserved in the sequence alignment (Fig. 4*a*). To assess their functional role, we designed six single point mutants: D35N, K118H, K118N, K118A, H34N and H34A. As shown in Fig. 5, D35N resulted in an almost complete loss of enzyme activity. This is consistent with the widely accepted mechanism that Asp35 directly participates in the protonation of isochorismate C3′. Replacement of Lys118 by His and Asn also resulted in a complete loss of enzymatic activity. Unexpectedly, the K118A mutant still had ∼30% activity. This shows that Lys118 is important for catalysis, but may not be absolutely required. Both H34N and H34A exhibited partial activity, suggesting that His34 plays an important but not essential role in catalysis.

3.5. Phenotype analysis of *vibB-ISC* mutants using the Δ*entB-ICL* strain

As reported by Liu *et al.* (1990), Rusnak *et al.* (1990) and Drake *et al.* (2006), EntB-ICL has the same function as VibB-ISC. For this reason, *E. coli* strain BL21 (DE3) with an *entB-ICL* deletion was used to analyze the phenotype of *vibB-ISC* mutants. As shown in Fig. 6, the viability of the Δ*entB-ICL* strain is greatly reduced upon the addition of 2,2-bipyridyl compared with the wild type, but can be rescued by expression of EntB-ICL or VibB-ICL. However, expression of VibB-ISC-K118H, VibB-ISC-K118N or VibB-ISC-D35N does not improve the viability of the Δ*entB-ICL* strain on an LB plate with 2,2-bipyridyl. The VibB-ISC-K118A strain grows better than the other VibB-ISC mutants, but not as well as the EntB-ICL and VibB-ISC strains. These results are consistent with our biochemical data.

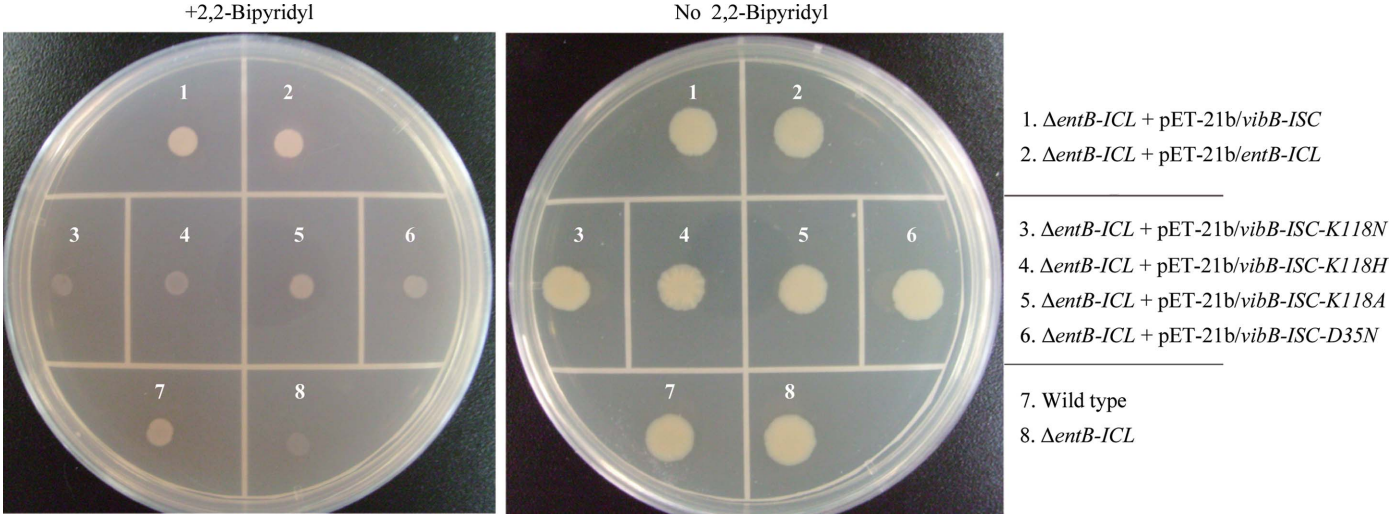

Figure 6
Phenotype characterization of *vibB-ISC* mutants. Serial dilutions of *E. coli* cultures were spotted onto LB plates with or without 2,2-bipyridyl.

Table 2
Summary of the MD simulation results.

(*a*) Hydrogen bonds between the catalytic waters and Asp35 in the MD simulation.

	WAT1		WAT2	
Asp35 OD···H WAT	Occurrence (%)	Distance (Å)	Occurrence (%)	Distance (Å)
WT	82.3	2.204 (0.460)	77.0	1.856 (0.267)
K118H	98.1	1.745 (0.243)	24.9	2.646 (0.653)
K118N	100.0	1.690 (0.127)	1.90	5.480 (1.268)
K118A	52.2	2.557 (0.699)	99.0	1.737 (0.283)

(*b*) Distance between WAT1 (O) and isochorismate (C2′) in the MD simulation.

	WT	K118H	K118N	K118A
Distance (ISC C2′··· O WAT1) (Å)	3.661 (0.285)	4.988 (0.545)	4.415 (0.261)	3.366 (0.207)

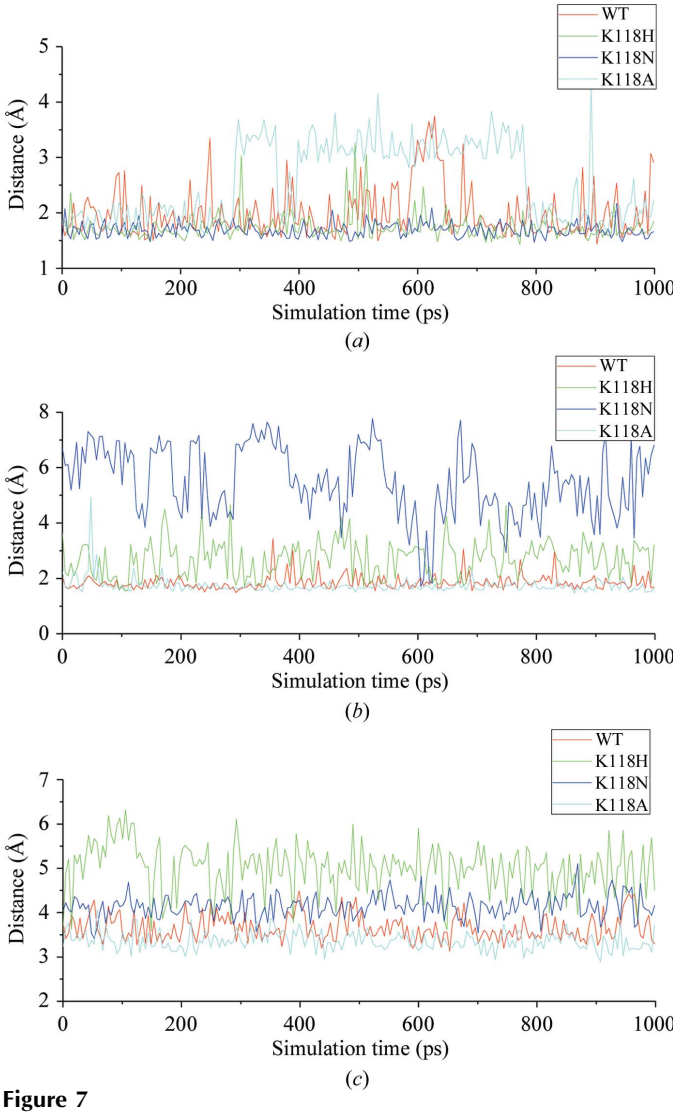

Figure 7
Time evolution of distances during MD runs. (*a*, *b*) Distances between the catalytic waters WAT1 (*a*) and WAT2 (*b*) and residue 118; (*c*) distances between the catalytic water WAT1 and the C2′ atom of isochorismate.

3.6. MD analysis of the water molecules adjacent to the active site

Our studies on VibB-ISC have suggested that the water molecules adjacent to the active site might play an vital role in vinyl ether hydrolysis catalyzed by isochorismatase. These studies are mainly based on the crystal structure of the catalytically inactive D35N mutant of VibB-ISC in complex with isochorismate. To ascertain the catalytic roles of the water molecules and their interaction with Lys118, we calculated the MD trajectories of the wild-type VibB-ISC complex structure and a series of mutants targeting Lys118, including K118A, K118H and K118N.

The time evolution of the C^{α}-atom r.m.s.d. of the instantaneous structures indicates that all systems reached equilibrium with respect to the r.m.s.d.s during the trajectory analysis (Supplementary Fig. S1). We also observed the local r.m.s.d. for residue 35, residue 118, isochorismate and the two adjacent water molecules, which may play vital roles in the catalysis. The average r.m.s.d. data also confirmed the stability of the final models and the reliability of the results of MD trajectory analysis (Supplementary Table S2).

Our studies indicated that the catalytic water (WAT1) might function as a general acid that protonates the Asp35 carboxylate prior to the protonation of isochorismate. As shown in Table 2(*a*), WAT2 forms hydrogen bonds to OD1 or OD2 of Asp35 in wild-type VibB-ISC and the K118A and K118H mutants which are not present in the crystal structure. As listed in Table 2(*a*), the hydrogen-bond occurrence involving WAT1 is >80% for wild-type VibB-ISC and the K118H and K118N mutants and ∼50% for the K118A mutant, indicating that the hydrogen bond between WAT1 and Asp35 is weakened in the K118A mutant with respect to the others. This is consistent with the time-evolution result that the distance in the K118A mutant is not as stable as in the others (Fig. 7*a*). The hydrogen-bond occurrence involving WAT2 is >75% for wild-type VibB-ISC and the K118A mutant but <25% for the K118H and K118N mutants, indicating that the hydrogen bonds between WAT2 and Asp35 are much weaker for the K118H and K118N mutants. This is also consistent with the time-evolution result of the corresponding distances (Fig. 7*b*).

Our crystal structure reveals that the catalytic water (WAT1) may perform a nucleophilic attack on the intermediate carbocation/oxocarbonium ion. In the resulting MD models, WAT2 is too distant from the isochorismate C2′ to perform a nucleophilic attack. Therefore, we focused on the distance between WAT1 and isochorismate C2′. The time evolution of the distance for all MD runs is depicted in Fig. 7(*c*). The average distance is <3.7 Å for wild-type VibB-ISC and the K118A mutant, whereas it is >4.4 Å for the K118H and K118N mutants (Table 2*b*).

4. Discussion

The most significant feature observed in the complex structure of VibB-ISC is the binding of water molecules in the active site. WAT1 is positioned in an appropriate location for

nucleophilic attack on the C2′ atom of the substrate. The overall structure is highly similar to the PhzD–isochorismate complex structure from *P. aeruginosa*, with a C^{α} r.m.s.d. of 0.667 Å. The geometry and location of the active-site residues are also very similar in VibB-ISC and PhzD. Structural and sequence-alignment results suggest that the isochorismatases might have similar mechanisms in catalyzing vinyl ether hydrolysis (Fig. 2*c* and Fig. 4*a*). Based on the PhzD complex structure, a general process for the catalysis of vinyl ether hydrolysis by VibB-ISC was proposed. However, the catalytic functions of some specific amino-acid residues and waters remained an open question. In our study, the high-resolution structures and related experimental results provide important clues to the catalytic roles of the catalytic waters, Asp35, Lys118 and His34 in the active site (Fig. 4*b*).

As inferred from the crystal structures, Asp35 might act as a direct proton donor to isochorismate C3′ because of its intermediate position and orientation. Proton donation is considered to be the rate-determining step in vinyl ether hydrolysis, apparently without exception (Chiang *et al.*, 1989; Burt *et al.*, 1987). Electrostatic stabilization of the intermediate carbocation/oxocarbonium ion by the resulting Asp35 carboxylate is expected to contribute to transition-state stabilization. The side chain of D35N is hydrogen bonded to the catalytic water (WAT1; Fig. 4*b*) with a distance of ∼3.0 Å, suggesting its crucial role in the stabilization of this water molecule. This is supported by the observation that no waters are adjacent to the active-site residues in the PhzD–isochorismate structure with a D35A mutation. In the simulation of wild-type VibB-ISC, hydrogen bonds were stably formed with an occurrence of >75% between WAT2 and residue 35 (Fig. 7*b* and Table 2*a*) which were not present in the D35N simulation results (Fig. 7*d*), indicating that the charge state of residue 35 has an indispensable effect on the proper position of WAT2. Taken together, we propose two possible effects that account for the interaction between Asp35 and the catalytic waters (Fig. 8). (i) The catalytic water (WAT1 or WAT2) may act as a general acid that protonates the Asp35 carboxylate prior to isochorismate protonation and (ii) the ionizable side chain of Asp35 may function as a general base which activates the water molecule (WAT1) to perform a nucleophilic attack on the intermediate carbocation/oxocarbonium ion. As shown in Fig. 5, the D35N mutation resulted in an almost complete loss of enzyme activity, suggesting that Asp35 is vital for vinyl ether hydrolysis. The result is also consistent with the plasmid complement results depicted in Fig. 6.

In both structures, Lys118 and Asp35 (or Asn35) are positioned on opposite sides of the catalytic water (WAT1; Fig. 4*b*) within hydrogen-bonding distance, forming an 'electrostatic sandwich' (Fig. 8), which may make it easier for the proton to transfer from the catalytic water to the Asp35 carboxylate. It was not expected that the K118H and K118N mutants would lose enzymatic activity completely while the K118A mutant still retained ∼30% activity. This interesting observation can be explained by our molecular-dynamics study. In the resulting MD models, the hydrogen-bond occurrence involving WAT1 is >80% for wild-type VibB-ISC and the K118H and K118N mutants, and ∼50% for the K118A mutant (Table 2*a*), which suggests that the side chain of residue 118 plays a crucial role in the stabilization of WAT1. As listed in Table 2(*a*), WAT2 forms hydrogen bonds to OD1 or OD2 of Asp35 in wild-type VibB-ISC and the K118A and K118H mutants which are not present in the K118N mutant simulation results, indicating that residue 118 may also have an important effect on the correct positioning of WAT2. In the resulting MD models, WAT2 is too far from the isochorismate C2′ to perform a nucleophilic attack on the intermediate

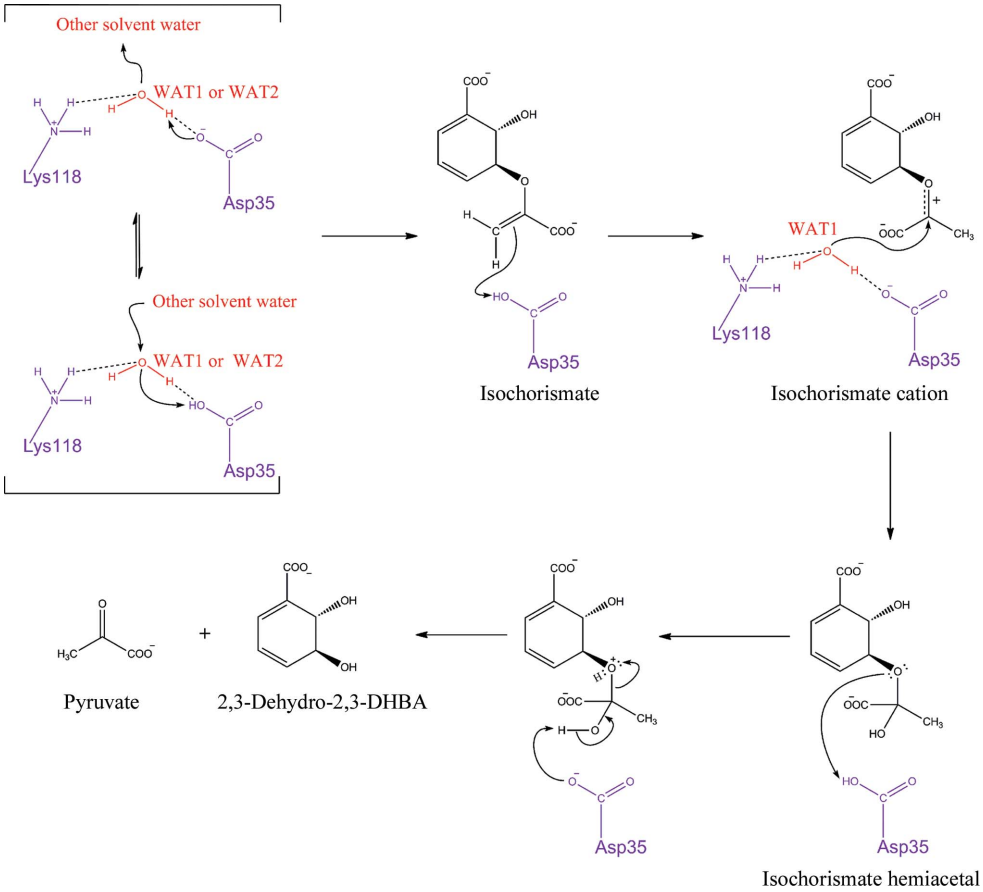

Figure 8
Representation of the proposed mechanism of isochorismate vinyl ether hydrolysis catalyzed by VibB-ISC. The water molecules participating in hydrolysis are shown in red; the catalytic residues are shown in purple.

carbocation/oxocarbonium ion. The time evolution of the distance between WAT1 and isochorismate C2′ is depicted in Fig. 7(*c*). The average distance is <3.7 Å for wild-type VibB-ISC and the K118A mutant, but is >4.4 Å for the K118H and K118N mutants (Table 2*b*). Our enzyme-assay results are consistent with the observation that the K118N and K118H mutants possess almost no measurable enzyme activity compared with wild-type VibB-ISC and the K118A mutant. The time evolution of the distances between WAT1 and residue 118 indicates that the catalytic water (WAT1) in the K118A mutant is not as stable as in wild-type VibB-ISC (Fig. 7*a*). This is also consistent with the enzyme-assay results showing that the K118A mutation resulted in an enzyme with ∼30% of the wild-type activity. These results are supported by the complementation of the Δ*entB-ICL* strain with plasmids for expression of the *vibB-ISC*, *vibB-ISC-K118N*, *vibB-ISC-K118H* and *vibB-ISC-K118A* genes, as shown in Fig. 6.

His34 may exert two roles in vinyl ether hydrolysis catalyzed by VibB-ISC as predicted from the crystal structures. Firstly, the hydrogen bond between His34 and Lys118 may assist in the proper orientation of Lys118. Secondly, His34 may form a hydrogen bond to Val146 to stabilize the Val146-Tyr147 *cis*-peptide bond, which is highly conserved in the isochorismatase family (Fig. 4*a*). However, both H34A and H34N exhibit partial activity, suggesting that His34 performs an important but not vital role in catalysis. Therefore, it seems unlikely that His34 participates in the protonation of isochorismate.

In summary, the catalytic waters may be involved in two reactions that contribute to vinyl ether hydrolysis (Fig. 8). Firstly, they may function as a general acid to protonate the Asp35 carboxylate prior to isochorismate protonation, which might be easier to perform *via* the 'electrostatic sandwich' mechanism described above. Secondly, the catalytic water (WAT1) may be activated by the ionizable Asp35 side chain to perform a nucleophilic attack on the intermediate carbocation/oxocarbonium ion. The positions of the two catalytic waters are both significantly affected by mutation of Asp35 and Lys118.

The genomic DNA of *V. cholerae* was a gift from Professor Bonnie Bassler. We thank Professor Qingsheng Qi for assistance in gene knockout. We thank the staff of beamline BL17U1 at the Shanghai Synchrotron Radiation facility for support with data collection. Dr Seth Parker, Clovis Unified School District is thanked for linguistic advice. This work was supported by the State Key Laboratory of Microbial Technology, Shandong University and Grant 2006AA02A324 from the Hi-Tech Research and Development Program of China.

References

Adams, P. D., Grosse-Kunstleve, R. W., Hung, L.-W., Ioerger, T. R., McCoy, A. J., Moriarty, N. W., Read, R. J., Sacchettini, J. C., Sauter, N. K. & Terwilliger, T. C. (2002). *Acta Cryst.* D**58**, 1948–1954.

Benkert, P., Tosatto, S. C. E. & Schomburg, D. (2008). *Proteins*, **71**, 261–277.

Berendsen, H. J. C., Postma, J. P. M., van Gunsteren, W. F. & Hermans, J. (1981). *Intermolecular Forces*, edited by B. Pullman, pp. 331–342. Dordrecht: Reidel.

Bowers, K. J., Chow, E., Xu, H., Dror, R. O., Eastwood, M. P., Gregersen, B. A., Klepeis, J. L., Kolossvary, I., Moraes, M. A., Sacerdoti, F. D., Salmon, J. K., Shan, Y. & Shaw, D. E. (2006). *SC 2006 Conference, Proceedings of the ACM/IEEE*, pp. 515–527. doi:10.1109/SC.2006.54.

Burt, R., Chiang, Y., Chwang, W., Kresge, A., Okuyama, T., Tang, Y. & Yin, Y. (1987). *J. Am. Chem. Soc.* **109**, 3787–3788.

Butterton, J. R., Choi, M. H., Watnick, P. I., Carroll, P. A. & Calderwood, S. B. (2000). *J. Bacteriol.* **182**, 1731–1738.

Chiang, Y., Chwang, W., Kresge, A. & Yin, Y. (1989). *J. Am. Chem. Soc.* **111**, 7185–7190.

Cristobal, S., Zemla, A., Fischer, D., Rychlewski, L. & Elofsson, A. (2001). *BMC Bioinformatics*, **2**, 5.

Darden, T., York, D. & Pedersen, L. (1993). *J. Chem. Phys.* **98**, 10089–10092.

Datsenko, K. A. & Wanner, B. L. (2000). *Proc. Natl Acad. Sci. USA*, **97**, 6640–6645.

Drake, E. J., Nicolai, D. A. & Gulick, A. M. (2006). *Chem. Biol.* **13**, 409–419.

Emsley, P. & Cowtan, K. (2004). *Acta Cryst.* D**60**, 2126–2132.

Griffiths, G. L., Sigel, S. P., Payne, S. M. & Neilands, J. B. (1984). *J. Biol. Chem.* **259**, 383–385.

Grosse-Kunstleve, R. W. & Adams, P. D. (2002). *J. Appl. Cryst.* **35**, 477–480.

Holm, L. & Sander, C. (1993). *J. Mol. Biol.* **233**, 123–138.

Hoover, W. G. (1985). *Phys. Rev. A*, **31**, 1695–1697.

Keating, T. A., Marshall, C. G. & Walsh, C. T. (2000). *Biochemistry*, **39**, 15522–15530.

Kresge, A. J., Leibovitch, M. & Sikorski, J. A. (1992). *J. Am. Chem. Soc.*, **114**, 2618–2622.

Lamzin, V. S. & Wilson, K. S. (1993). *Acta Cryst.* D**49**, 129–147.

Laskowski, R. A., MacArthur, M. W., Moss, D. S. & Thornton, J. M. (1993). *J. Appl. Cryst.* **26**, 283–291.

Liu, J., Quinn, N., Berchtold, G. A. & Walsh, C. T. (1990). *Biochemistry*, **29**, 1417–1425.

Matthews, B. W. (1968). *J. Mol. Biol.* **33**, 491–497.

McCoy, A. J., Grosse-Kunstleve, R. W., Adams, P. D., Winn, M. D., Storoni, L. C. & Read, R. J. (2007). *J. Appl. Cryst.* **40**, 658–674.

Merritt, E. A. (1999). *Acta Cryst.* D**55**, 1997–2004.

Miethke, M. & Marahiel, M. A. (2007). *Microbiol. Mol. Biol. Rev.* **71**, 413–451.

Neilands, J. B. (1995). *J. Biol. Chem.* **270**, 26723–26726.

Nosé, S. (1984). *Mol. Phys.* **52**, 255–268.

Otwinowski, Z. & Minor, W. (1997). *Methods Enzymol.* **276**, 307–326.

Parsons, J. F., Calabrese, K., Eisenstein, E. & Ladner, J. E. (2003). *Biochemistry*, **42**, 5684–5693.

Ramachandran, G. & Sasisekharan, V. (1968). *Adv. Protein Chem.* **23**, 283–438.

Romão, M. J., Turk, D., Gomis-Rüth, F. X., Huber, R., Schumacher, G., Möllering, H. & Rüssmann, L. (1992). *J. Mol. Biol.* **226**, 1111–1130.

Rusnak, F., Liu, J., Quinn, N., Berchtold, G. A. & Walsh, C. T. (1990). *Biochemistry*, **29**, 1425–1435.

Ryckaert, J. P., Ciccotti, G. & Berendsen, H. J. C. (1977). *J. Comput. Phys.* **23**, 327–341.

Wibbenmeyer, J., Brundage, L., Padgette, S. R., Likos, J. J. & Kishore, G. M. (1988). *Biochem. Biophys. Res. Commun.* **153**, 760–766.

Winn, M. D. *et al.* (2011). *Acta Cryst.* D**67**, 235–242.

Word, J. M., Lovell, S. C., Richardson, J. S. & Richardson, D. C. (1999). *J. Mol. Biol.* **285**, 1735–1747.

Wyckoff, E. E., Smith, S. L. & Payne, S. M. (2001). *J. Bacteriol.* **183**, 1830–1834.

Wyckoff, E. E., Stoebner, J. A., Reed, K. E. & Payne, S. M. (1997). *J. Bacteriol.* **179**, 7055–7062.

Young, I., Batterham, T. & Gibson, F. (1969). *Biochim. Biophys. Acta*, **177**, 389–400.